Journal Name

ARTICLE

Molecular Engineering of Enamine-Based Small Organic Compounds as Hole-Transporting Materials for Perovskite Solar Cells

Maryte Daskeviciene,[†a] Sanghyun Paek,[†b] Artiom Magomedov,[a] Kyoung Taek Cho,[b] Michael Saliba,[c] Ausra Kizeleviciute,[a] Tadas Malinauskas,[a] Alytis Gruodis,[d] Vygintas Jankauskas,[d] Egidijus Kamarauskas,[d] Mohammad Khaja Nazeeruddin,[*b] and Vytautas Getautis[*a]

Search for the new classes of the hole transporting materials (HTMs) is a very important task on the way towards commercialization of the perovskite solar cells (PSCs). In this work, synthesis, and performance in PSCs of a new enamine-based HTMs are presented. Synthesis scheme is very short, consisting of only one step, starting from the commercially available aromatic amines. Moreover, the reaction does not require metal catalyzers and is based on the condensation chemistry with the water as a by-product. It was shown that PSCs with such materials reach high power conversion efficiency (PCE), with the highest PCE of 19% achieved for the **V1021**-based device. This work establishes enamines as a very promising class of materials for the application in PSCs.

Introduction

Due to their outstanding properties, hybrid organic-inorganic perovskite materials have shown great potential for use in photovoltaics, thermoelectricity, light-emitting diodes, lasers, plasmonics, field-effect transistors, photodetectors, and sensors [1–7]. Within a few years, they have revolutionized the photovoltaic field leading to device efficiencies of more than 23% [8,9]. Typical perovskite solar cell (PSC) configuration consists of a multi-layered stack where the perovskite is sandwiched in between an electron-transporting layer, usually TiO_2, and an organic hole-transporting material (HTM). HTM-free device configuration has also been extensively investigated, however, it is still a subject of ongoing research and the highest efficiency of 10.49% for devices with the gold electrode[10,11] and 16% for the carbon electrode devices[12] has been achieved. Currently, costly 2,2`,7,7`-tetrakis(*N*,*N*-di-*p*-methoxyphenylamine)-9,9`-spirobifluorene (Spiro-OMeTAD) is the most widely used small molecule HTM to obtain high efficiency devices[13–15]. However, the tedious synthetic procedures and purification processes of this HTM make it cost ineffective and thus limit its application

a. *Department of Organic Chemistry, Kaunas University of Technology, Radvilenu pl. 19, 50254, Kaunas, Lithuania. E-mail: vytautas.getautis@ktu.lt*
b. *Group for Molecular Engineering of Functional Materials, Institute of Chemical Sciences and Engineering, École Polytechnique Fédérale de Lausanne, Rue de l'Industry 17, CH-1951, Sion, Switzerland. E-mail: mdkhaja.nazeeruddin@epfl.ch*
c. *Adolphe Merkle Inst, Chemins Verdiers 4, CH-1700 Fribourg, Switzerland*
d. *Institute of Chemical Physics Vilnius University, Sauletekio al.3, Vilnius LT-10257, Lithuania*
† M.D. and S.P. contributed equally to this work.
Electronic Supplementary Information (ESI) available: experimental procedures, theoretical calculations, device fabrication details etc. See DOI: 10.1039/x0xx00000x

and commercialization[16]. Moreover, the study by Binek et al. has shown that Spiro-OMeTAD can significantly contribute to the overall cost of materials required for the manufacturing of high-performance devices[17]. To engineer small molecule HTMs which are considerably cheaper than Spiro-OMeTAD, shorter reaction schemes with simple purification procedures are required. Successful examples include azomethine-[18], hydrazone-based[19] HTMs, methoxydiphenylamine substituted fluorene[20,21] and bifluorenylidene-based derivatives[22], spiro[fluorene-9,9`-xanthene]-based materials[23–25], and methoxydiphenylamine substituted branched carbazole derivatives[26–28].

Recently, we have reported a simple carbazole-based conjugated enamine named V950, which resulted in impressive power conversion efficiencies (PCE) of 17.8%[29] and is comparable to the state-of-the-art material Spiro-OMeTAD on a like-to-like comparison. This new small-molecule hole conductor was prepared from commercially available 3-amino-9-ethyl-9*H*-carbazole in one step synthesis without the use of expensive catalysts, column chromatography or sublimation purification, simplifying product workup and therefore drastically reducing the preparation cost ($ 5.58 per gram)[29].

Herein, we report a synthesis of a whole series of enamine molecules based on the V950 model in order to conduct a more thorough investigation of this very promising structural concept and test the new HTM's with the state-of-the-art perovskite composition. The influence of aliphatic substituents 9-(2-ethyl)hexyl (**V1000**), 9-butyl (**V1013**), 9-hexyl-6-*tert*-butyl (**V1004**), and additional enamine moiety (**V1020**) on the thermal, optical, and photophysical properties of HTMs bearing carbazolyl chromophore were investigated. In addition, the
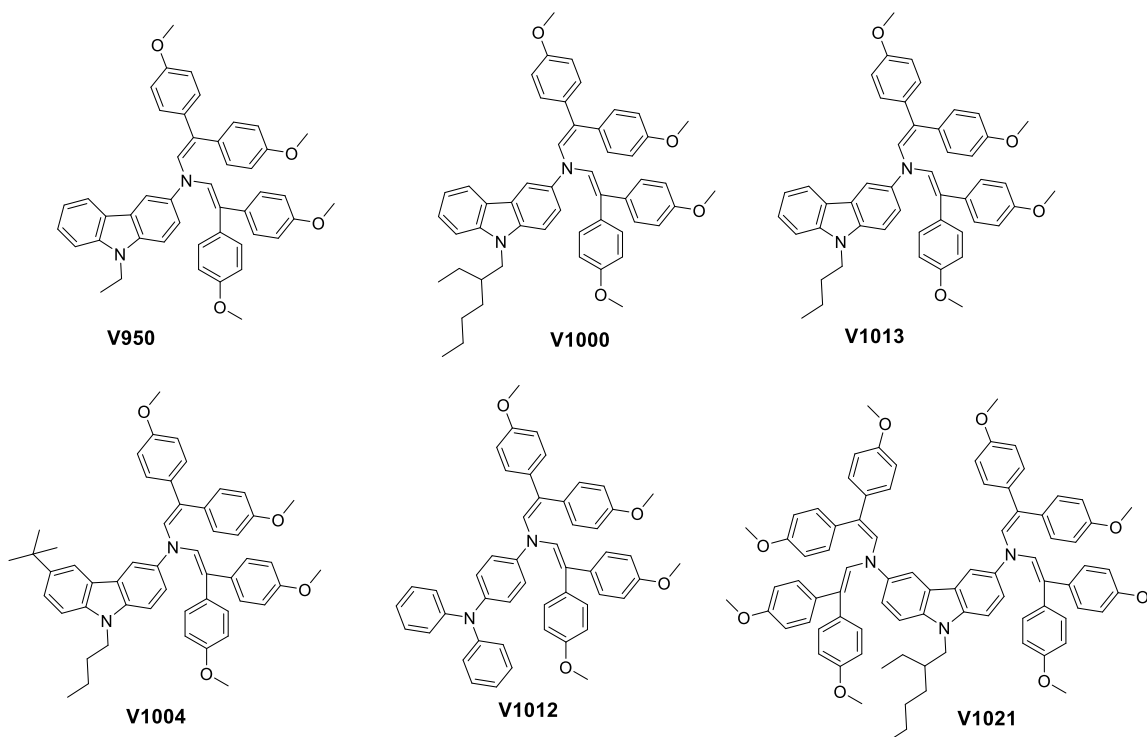

Figure 1. Structures of investigated enamine-based HTMs

Journal Name

ARTICLE

enamine-based HTM **V1012** bearing another, widely used for the synthesis of HTMs, triphenylamine chromophore[30] was synthesized and perovskite solar cells, utilizing n–i–p mesoporous configuration with triple-cation perovskite[31] and the new HTMs, were constructed and characterized.

Results and discussion

Synthesis

With the aim to investigate structural effects on the photophysical and electrical properties, as well as performance in PSCs, a series of the carbazole-based enamine derivatives **V1000**, **V1013**, **V1004**, and **V1021** was synthesized (Scheme 1). Enamine condensation chemistry offers an extremely simple route towards extended π-conjugated molecules[32]. The reaction can be performed under ambient conditions and water is the only by-product making product purification uncomplicated. A Dean-Stark trap is used to separate this water from the reaction mixture and thus the formation of the desired products is accelerated and the reaction duration reduces considerably. Initially, reactions of commercially available aromatic amino precursors, 9-(2-ethyl)hexyl-, 9-butyl-, 9-hexyl-6-*tert*-butyl 3-aminocarbazoles, 4-aminotriphenylamine, with 2,2-bis(4-methoxyphenyl)-acetaldehyde in the presence of (+/-)camphor sulfonic acid (CSA) were carried out and resulted in formation of the corresponding HTMs **V1000**, **V1013**, **V1004**, and **V1012** in moderate yields (47-57%) (Scheme 1a). The column chromatography was used to isolate the above mentioned HTMs and this is the main difference of the preparation method from the one described for the model HTM V950[29]. The same strategy was employed for the synthesis of the HTM possessing four enamine branches (**V1021**) from 9-(2-ethylhexyl)-9*H*-carbazole-3,6-diamine (Scheme 1b), only the double amount of 2,2-bis(4-methoxyphenyl)acetaldehyde was used in this case. The chemical structures of the synthesized products were verified by ^{1}H/^{13}C NMR spectroscopy and elemental analysis. All synthesized new enamine-based HTMs are soluble in common organic solvents such as chloroform, THF, or chlorobenzene, which are typically used for deposition of the hole transporting layer in PSCs. Detailed synthesis procedure and analysis can be found in the ESI.

Computational Study

To establish the most probable molecular structure, quantum chemical simulations of V950, **V1000**, **V1004**, **V1013**, **V1012**, and **V1021** were performed by means of Gaussian 09[33] package using density functional theory (DFT) method B3LYP. Optimization of the ground state geometry was done using 6–31G(d) basis set supplemented with polarization functions (Table S2). In Table S3, dipole moments of optimized molecular structures are presented. For the materials V950, **V1000**, **V1004**, **V1013** with different aliphatic fragments, only negligible changes of spatial orientation of enamine-substituents take place. Generally, enamine-substituents create V-shaped spatial
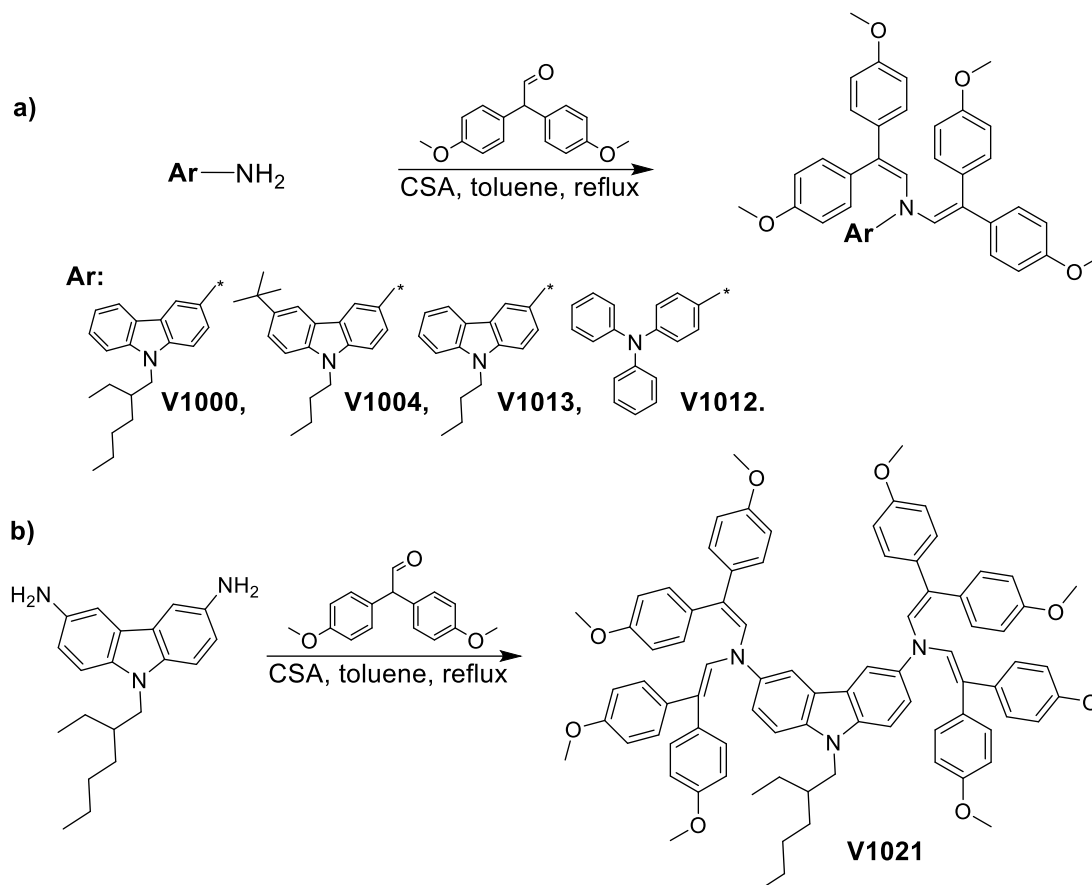
Scheme 1. The general scheme for the synthesis of the enamine-based HTMs: a) **V1000**, **V1004**, **V1013**, and **V1012**; b) **V1021**.

orientation of phenyl fragments with interfragmental angle close to the 120 degrees (between the long axis of phenyl, when phenyls are non-face-to-face-oriented in pair). Due to the possibility to obtain the big number of conformational motion (rotating about [>N–C=] junction), the strong position of fragmental substituents cannot be established. For **V1012** and **V1021**, the same V-shaped orientation of phenyl rings is observed.

Table S4 represents energies of electronic excitations ($S_0 \rightarrow S_n$) and corresponding oscillator strengths f_n of V950, **V1000**, **V1004**, **V1013**, **V1012,** and **V1021** compounds. Excited singlet states S_1, S_2, S_3 were simulated by *Gaussian09* by means of the semi-empirical time-dependent (TD) method. Transition $S_0 \rightarrow S_1$ is forbidden for all carbazole-based compounds and partially-allowed for triphenylamine-based compound (**V1012**). Transition $S_0 \rightarrow S_2$ is partially-allowed for all compounds.

Spatial distributions of electron density for the highest occupied molecular orbital (HOMO) and next HOMO as well as the lowest unoccupied molecular orbital (LUMO) and next LUMO were obtained using TD routine and are presented in Table S5-S10. A more detailed description is available in ESI.

Thermal Properties

Thermal properties of the synthesized compounds were investigated by thermal gravimetric analysis (TGA) and differential scanning calorimetry (DSC) methods (Table 1). The results are presented in Figure 2 and the full characteristics are provided in Table 1. TGA analysis has shown that all synthesized compounds show good thermal stability up to ~400 °C, that is comparable with model compound V950 (T_{dec} = 380 °C[29]) and slightly lower than that of Spiro-OMeTAD (T_{dec} = 449 °C[34]). The lowest 5% weight loss temperature of 370 °C is observed for compound **V1004** possessing *tert*-butyl group attached to the carbazolyl chromophore; however, it is high enough to signify good thermal stability, which is required for photovoltaic devices. In addition, a rapid weight loss during TGA experiments, which indicates that enamine-based HTMs undergo sublimation rather than thermal decomposition, are observed. This suggests that these HTMs could also be processed by vacuum process which would further widen their applications.

The results of DSC analysis have revealed that **V1000**, **V1012**, and **V1013**, similarly as V950 and Spiro-OMeTAD, can exist both in the crystalline and amorphous state while others have a stronger tendency to crystallize. During the first heating, only melting is detected (Figure 2b, Table 1). No crystallization takes place during cooling or second heating scans. Only glass transition (T_g) of these compounds was registered during the second heating, what is desired to form uniform HTM films in PSCs. Additional *tert*-butyl (**V1004**) and enamine moieties
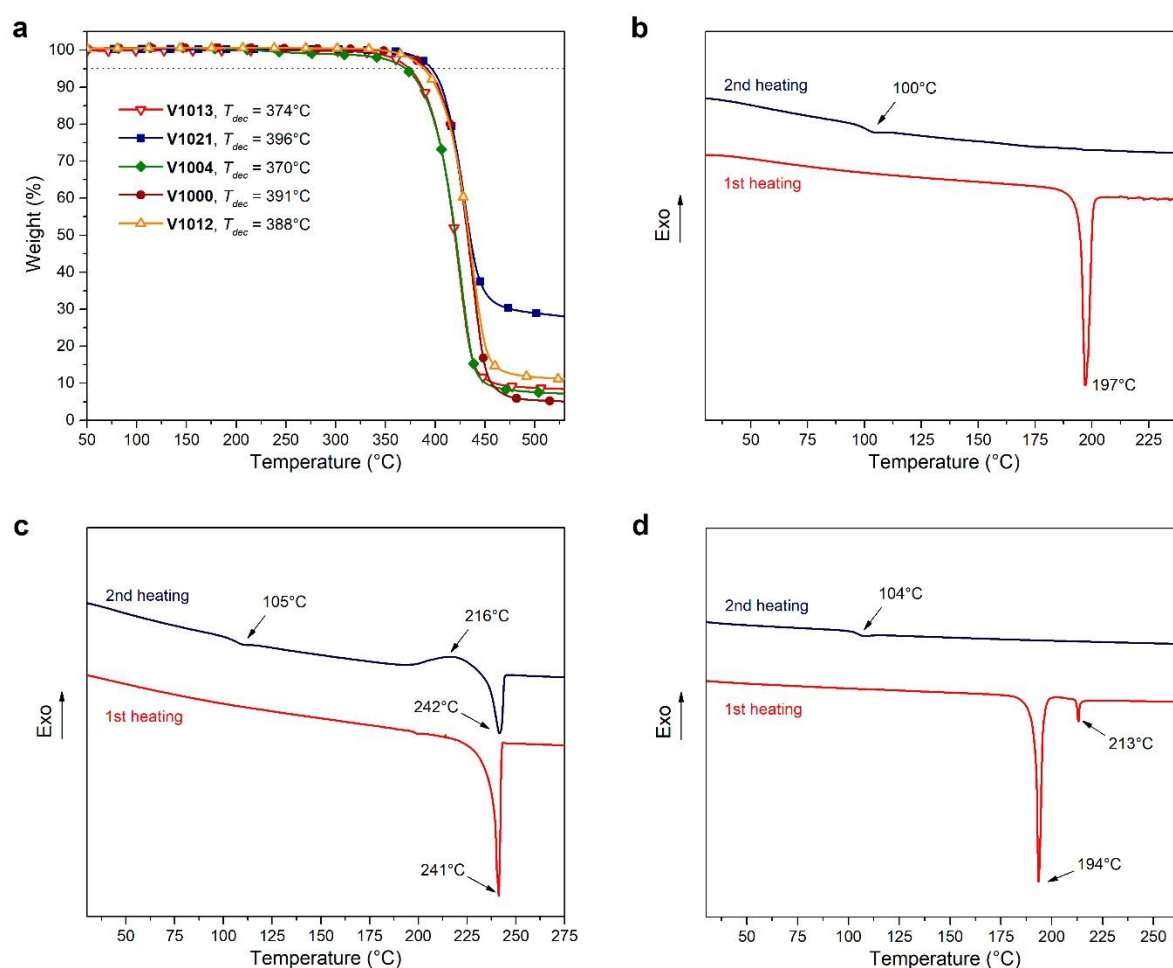
Figure 2. (a) TGA heating curves of new HTMs (heating rate 10 K min^{-1}). DSC heating curves of (b) **V1013**, (c) **V1004**, (d) **V1012 (**heating and cooling rate 10 K min^{-1}).

(**V1021**) affect the thermal properties of HTMs bearing carbazolyl chromophore: during second heating glass transition is observed followed by recrystallization at 105 °C and 132 °C, respectively. Interestingly, the DSC curve for **V1012** at first heating reveals two peaks, corresponding to two eutectic melting points at 194 °C and 213 °C. Thus, triphenylamine core-based enamine is distinguished by polymorphism with the predominant second crystalline phase at 194 °C.

Table 1. Thermal properties of the enamine-based HTMs and Spiro-OMeTAD[34]

HTM	T_m [ºC][a)]	T_{recr} [ºC]	T_g [ºC][b)]	T_{dec} [ºC]
V950	227	–	111	383
V1000	205	–	85	391
V1004	241	216[b)]	105	370
V1012	194, 213	–	104	388
V1013	197	–	100	374
V1021	266	176[a)], 198[b)]	132	396
Spiro-OMeTAD	245	–	125	449

Determined by DSC: scan rate, 10 K min^{-1}; N$_2$ atmosphere; [a)]first run; [b)]second run.

Optical Properties

The UV-vis absorption bands of the carbazole core-based enamines **V1000**, **V1013**, **V1004**, **V1021**, and triphenylamine core-based enamine **V1012** measured in THF are shown in Figure 3. The spectra of the model HTM V950, as well as parent compounds 3-amino-9-ethylcarbazole and 4-amino-triphenylamine, are given for comparison reasons. As expected, the 9- and 3-alkylated carbazole core-based enamines **V1000**, **V1013**, and **V1004** absorb in a similar region as V950 and consist of a weak band in the long wavelength region (~ 400 nm) due to n–π* followed by a broad and intense band in the UV region (330 nm) due to π–π* transitions. The π–π* absorption bands for these HTMs are bathochromically shifted with respect to the reference 3-amino-9-ethylcarbazole by 30 nm, indicating an increase in the size of the π-conjugated system due to carbazole core engineering by enamine moieties possessing 4-methoxyphenyl side arms. Obviously, this is more expressed in the case of triphenylamine core-based enamine **V1012** as the π–π* absorption band is bathochromically shifted by 50 nm. Furthermore, HTM possessing four enamine branches (**V1021**),

as compared to **V1000** possessing two enamine branches, shows both the hyperchromic effect and bathochromic shift to longer wavelengths due to the expanded conjugated π-electrons system.
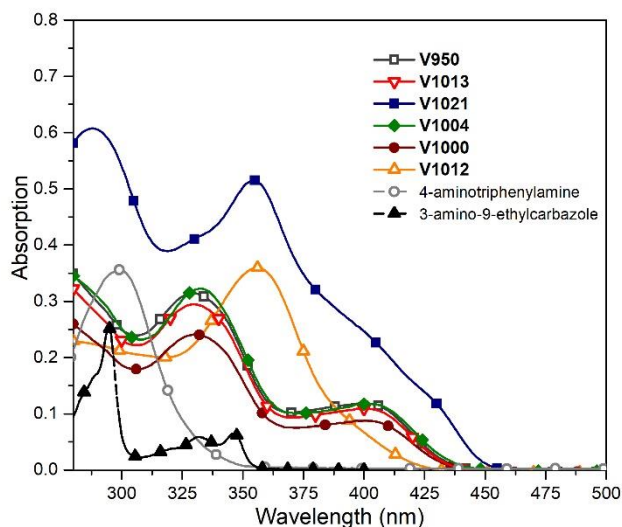

Figure 3. UV–vis absorption spectra of enamine-based HTMs, 3-amino-9-ethylcarbazole, and 4-aminotriphenylamine

Photoelectrical Properties

One of the important parameters of the HTMs, that need to be taken into consideration before constructing a device, is a solid-state ionization potential (I_p), which gives an accurate estimation of the highest occupied molecular orbital (HOMO) energy level of HTMs. The ionization potentials of the novel HTMs were measured by photoelectron spectroscopy in air (PESA) technique and results are presented in Figure S1 and Table 2; the measurement error is evaluated as 0.03 eV. The compounds with the carbazole core and different alkyl fragments (V950, **V1000**, **V1013**) have almost the same I_p values of 5.01 eV, 5.00 eV, and 4.97 eV respectively. Compound **V1004** possessing *tert*-butyl group attached to the carbazolyl chromophore has slightly higher I_p value of 5.08 eV. The highest I_p value was measured for enamine-based HTM with triphenylamine core **V1012** (5.11 eV). On the other hand, incorporation of the four enamine fragments resulted in the lowest I_p of 4.93 eV for **V1021**. The estimated I_p values are very close to the value of the model HTM V950[29] and Spiro-OMeTAD (5.00 eV)[34] and are suitable for application in perovskite solar cell devices to ensure efficient hole transfer at the interface.

Another important property is the ability of the HTM to transport holes, which can be quantified by measuring hole drift mobility. The results of measurements of hole drift mobility by means of xerographic time of flight (XTOF) technique are presented in Table 2 and Figure 4. At the low electrical fields, all materials show hole drift mobilities in the same order of magnitudes, and slightly lower than that of the Spiro-OMeTAD. Change of the carbazole chromophore to the triphenylamine in **V1012** did not lead to substantial changes in the hole drift mobility, however, it is less dependent on the field strength.

Incorporation of the aliphatic groups have not strongly affected mobilities, and the mobility values μ_0 are almost the same for **V950**, **V1000**, **V1004**, and **V1013**. On the other hand, enamine **V1021** with four enamine branches shows the highest charge transporting ability, reaching μ_0 of $5.9 \cdot 10^{-5}$ cm^2 V^{-1} s^{-1}. These measurements further suggest that materials would be able to efficiently collect charges in the PSCs. While there is no strong correlation between hole drift mobility and device performance, usually higher values are required to achieve high PCE.

To evaluate charge extraction ability of the newly synthesized HTMs, steady-state photoluminescence spectroscopy measurements were conducted. All materials showed significantly reduced PL of the perovskite layer, which is commonly attributed to the efficient extraction of the holes.

Table 2. Hole drift mobility and I_p data of the enamine-based HTMs and Spiro-OMeTAD[22,34]

HTM	μ_0 [cm^2 V^{-1} s^{-1}][a]	μ [cm^2 V^{-1} s^{-1}][b]	I_p [eV][c]
V950	$1.9 \cdot 10^{-5}$	$1.5 \cdot 10^{-3}$	5.01
V1000	$3.2 \cdot 10^{-5}$	$9.0 \cdot 10^{-4}$	5.00
V1004	$1.2 \cdot 10^{-5}$	$4.6 \cdot 10^{-4}$	5.08
V1012	$2.6 \cdot 10^{-5}$	$4.9 \cdot 10^{-4}$	5.11
V1013	$1.3 \cdot 10^{-5}$	$5.5 \cdot 10^{-4}$	4.97
V1021	$5.9 \cdot 10^{-5}$	$2.1 \cdot 10^{-3}$	4.93
Spiro-OMeTAD	$1.3 \cdot 10^{-4}$	$5.2 \cdot 10^{-3}$	5.01

Mobility value at [a]zero field strength; [b]$6.4 \cdot 10^5$ V cm^{-1} field strength; [c]I_p was measured by the photoemission in air method from films.

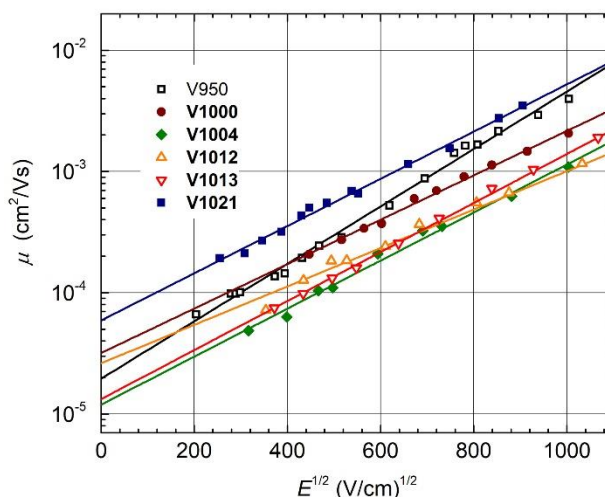**Figure 4.** Electric field dependencies of the hole-drift mobility (μ) of the investigated enamines V950, **V1000**, **V1004**, **V1012**, **V1013**, and **V1021**

Perovskite Solar Cells

To test operational performance of the synthesized HTMs, PSCs of mesoporous architecture (FTO/TiO$_2$/m.p.TiO$_2$/SnO$_2$/Cs$_{0.1}$(MA$_{0.15}$FA$_{0.85}$)$_{0.9}$Pb(I$_{0.85}$Br$_{0.15}$)/HTM/Au) were constructed and investigated. The detailed fabrication procedure can be found in SI. Performance of the

new HTMs was compared to that of the devices with V950 and Spiro-OMeTAD.

First, we compared the performance of the new HTMs with that of the model compound V950. All devices showed good performance and weak hysteresis (Figure S4). For the **V1021**-based device, almost no hysteresis was observed. As seen from the data in Figure 5a and Table 3, all of them have almost the same short-circuit current density (J_{sc}) values, which are in the range from 22.4 mA/cm^2 for **V1013** to 22.6 mA/cm^2 for **V1012**. This suggests that HTMs does not strongly affect charge collection properties of the perovskite, as can be seen from the incident photon-to-current efficiency (IPCE) spectra (Figure S5). Fill-factor (*FF*) also differs only slightly for the majority of the devices, with the exception of **V1000**, for which lower *FF* of 71% was obtained. However, the main variation of the performance stems from the changes in open-circuit voltage (V_{oc}). Overall, three out of five new compounds outperformed V950, reaching 19% for **V1012** and **V1021**, and 18.6% for **V1004**.

Comparison of the performance of the materials containing different aliphatic substituents has revealed that in two cases introduction of the insulating chains reduces performance (16.5% for **V1000** and 17.1% for **V1013**), however in case of **V1004** performance is on the same level as the one of V950, even though the μ_0 value for this HTM is the lowest among studied materials. It emphasizes the importance of the substituent at the 6 position of the carbazole fragment. Change of the chromophore from carbazole to triphenylamine led to the slightly better performance (19.0% for **V1012**). The slight increase was observed for all three parameters, in comparison to V950, resulting in an overall 0.6% PCE increase. It illustrates a possibility to further expand this synthetical strategy to the other photoactive fragments. Another compound, reaching 19.0%, was **V1021** with a double number of enamine chromophores, mainly due to the increase in V_{oc}. As in the case of V1004, 6 position of carbazole is substituted, however, in this case with the redox-active moiety. Such a change in structure led to the best performance among new HTMs. For **V1021**, the highest PCE coincides with the highest hole drift mobility value, measured for the enamine HTMs (Table 2).

In a Figure S8 maximum power point tracking of the fresh devices is presented. It can be seen, that general trend in performance is preserved. In addition, comparison of the best-performing devices is confirmed by statistical data (Figure S6).

Table 3. Solar cell performance parameters, extracted from J-V curves.

HTM	J_{sc} [mA/cm^2]	V_{oc} [V]	*FF* [%]	PCE [%]
V950	22.5	1.081	75.7	18.40
V1000	22.46	1.036	71.0	16.51
V1004	22.49	1.093	75.7	18.61
V1012	22.64	1.095	76.6	18.98
V1013	22.39	1.022	74.7	17.09
V1021	22.62	1.118	75.2	19.01
Spiro-OMeTAD	22.5	1.125	75.5	19.10

In Figure 5b, the comparison between best-performing enamine **V1021**, V950, and Spiro-OMeTAD is presented. While V950 shows slightly lower V_{oc} (1.081 V) than that of Spiro-OMeTAD (1.125 V), an increased number of the enamine moieties leads to the highest drift mobility values of $\mu_0 = 5.9 \cdot 10^{-5}$ cm^2 V^{-1} s^{-1}. and higher V_{oc} (1.118 V). This improvement leads to the same performance as the one of Spiro-OMeTAD-based devices.

Another important topic is device stability. Evaluation of the shelf life-time is presented in Figure 6. Overall, PCE of all HTMs increased slightly over the first 30 days. Afterward, some degradation started to occur, with the most pronounced drop in efficiency for **V1000**, for which PCE reduced to 85% after 80 days. Stability of all other HTMs was comparable to that of V950 (>98% after 80 days) and was slightly better than that of Spiro-OMeTAD (95% after 80 days), which is on par with our recent study of the enamine-based HTMs[35]. For the **V1000** the drop in performance was the most pronounced. The reason might be in the lowest T_g of the **V1000**, which could lead to the spontaneous crystallization even at lower temperatures, and as a consequence to the reduced performance[34]. Interestingly, the performance of the device with **V1021** was still slightly rising (in
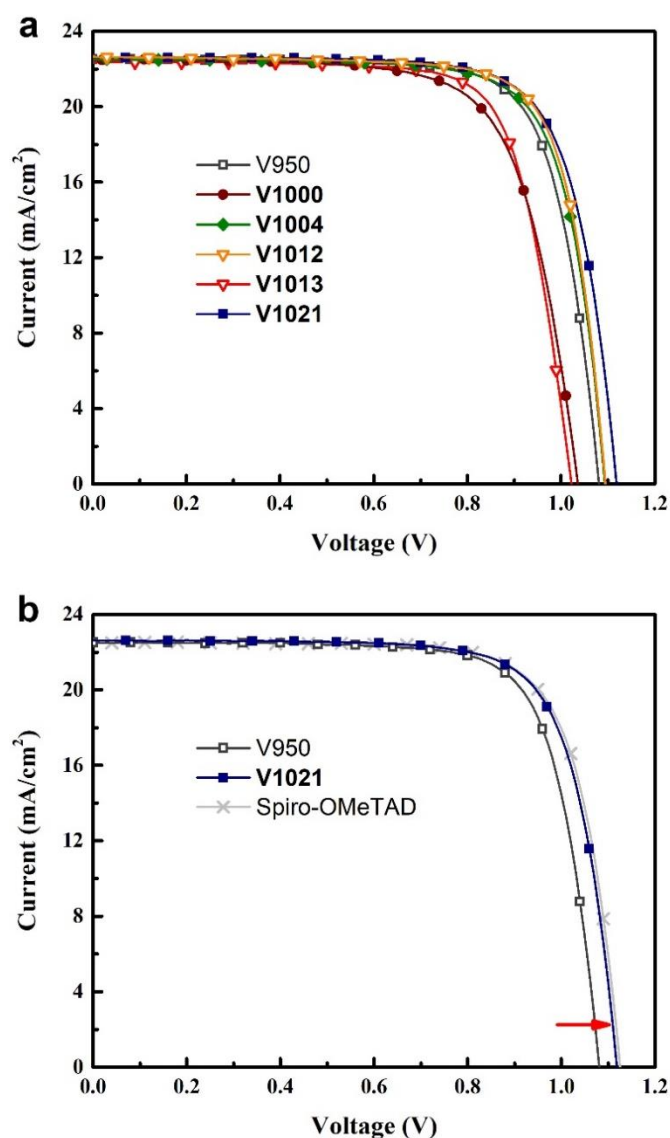
Figure 5. (a) J–V characteristics of best-performing enamines V950, **V1000**, **V1004**, **V1012**, **V1013**, and **V1021**; (b) comparison of J–V characteristics of the best performing V950, **V1021**, and Spiro-OMeTAD

a range of ~1%) even after 80 days, what in a combination with the best performance makes this HTM very promising for the further investigations.
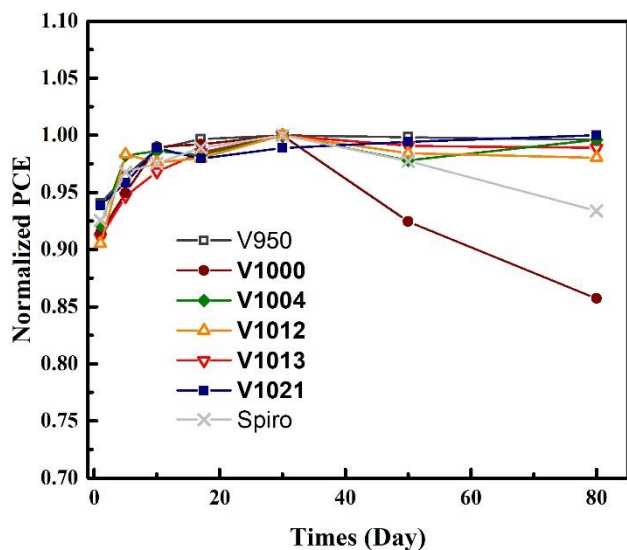

Figure 6. Stability test without encapsulation (relative humidity around 20%) of the PSCs with V950, **V1000**, **V1004**, **V1012**, **V1013**, **V1021**, and Spiro-OMeTAD. The devices were measured under 1 sunlight illumination and kept at room temperature in the dark until the next measurement.

Conclusions

In conclusion, 5 new enamine-based HTMs were synthesized by metal-free enamine condensation reaction and tested for the performance in PSCs. Materials are thermally stable and could be deposited by a vacuum process. HTMs have I_p in a range of $4.97 - 5.10$ eV, which is suitable values for the application in PSCs. Hole drift mobility values at the low electrical fields are of the 10^{-5} cm² V⁻¹ s⁻¹ order of magnitude, reaching the highest value of $5.9 \cdot 10^{-5}$ cm² V⁻¹ s⁻¹ for **V1021** with four enamine branches. PSCs with new HTMs showed very good performance, the best efficiency reaching 19.0% PCE for **V1021**, which is on par with that of the state-of-the-art material Spiro-OMeTAD (19.1%). Moreover, **V1004**, **V1012**, **V1013**, and **V1021** showed superior device stability, outperforming Spiro-OMeTAD. This work lays a foundation for the further studies of the enamine-based molecules, e.g. by increasing amount of the enamine branches, or by use of the different central fragment (thiophene, indole etc.).

Conflicts of interest

There are no conflicts to declare.

Acknowledgments

Author Contributions

V.G., M.K.N. conceived the initial idea and supervised the research. M.D. contributed to the design, discussion, and improvement of all experiments. A.K. conducted the synthesis and structural characterization of the compounds. M.S., S.P., and K.T.C. performed the fabrication and characterization of solar cells. T.M., A.M. carried out the DSC, TGA, UV-Vis-NIR lights absorption measurements. E.K., V.J. carried out the ionization potential and charge mobility measurements. A.G. carried out the quantum chemical simulations of HTMs. All authors contributed to writing this paper.

References

1   H. J. Snaith, *Nat. Mater.*, 2018, **17**, 372–376.
2   Y. He and G. Galli, *Chem. Mater.*, 2014, **26**, 5394–5400.
3   M. Saliba, S. M. Wood, J. B. Patel, P. K. Nayak, J. Huang, J. A. Alexander-Webber, B. Wenger, S. D. Stranks, M. T. Hörantner, J. T.-W. Wang, R. J. Nicholas, L. M. Herz, M. B. Johnston, S. M. Morris, H. J. Snaith and M. K. Riede, *Adv. Mater.*, 2016, **28**, 923–929.
4   M. Saliba, W. Zhang, V. M. Burlakov, S. D. Stranks, Y. Sun, J. M. Ball, M. B. Johnston, A. Goriely, U. Wiesner and H. J. Snaith, *Adv. Funct. Mater.*, 2015, **25**, 5038–5046.
5   S. A. Veldhuis, P. P. Boix, N. Yantara, M. Li, T. C. Sum, N. Mathews and S. G. Mhaisalkar, *Adv. Mater.*, 2016, **28**, 6804–6834.
6   J. Sun, J. Wu, X. Tong, F. Lin, Y. Wang and Z. M. Wang, *Adv. Sci.*, 2018, **5**, 1700780.
7   K. Wang, G. Li, S. Wang, S. Liu, W. Sun, C. Huang, Y. Wang, Q. Song and S. Xiao, *Adv. Mater.*, 2018, **30**, 1801481.
8   N. J. Jeon, H. Na, E. H. Jung, T.-Y. Yang, Y. G. Lee, G. Kim, H.-W. Shin, S. Il Seok, J. Lee and J. Seo, *Nat. Energy*, 2018, **3**, 682–689.
9   NREL efficiency chart, https://www.nrel.gov/pv/assets/images/efficiency-chart.png, (accessed 6 February 2018).
10 L. Etgar, P. Gao, Z. Xue, Q. Peng, A. K. Chandiran, B. Liu, M. K. Nazeeruddin and M. Grätzel, *J. Am. Chem. Soc.*, 2012, **134**, 17396–17399.
11 J. Shi, J. Dong, S. Lv, Y. Xu, L. Zhu, J. Xiao, X. Xu, H. Wu, D. Li, Y. Luo and Q. Meng, *Appl. Phys. Lett.*, 2014, **104**, 63901.
12 H. Zhang, H. Wang, S. T. Williams, D. Xiong, W. Zhang, C. C. Chueh, W. Chen and A. K.-Y. Jen, *Adv. Mater.*, 2017, **29**, 1606608.
13 S. Ameen, M. A. Rub, S. A. Kosa, K. A. Alamry, M. S. Akhtar, H.-S. Shin, H.-K. Seo, A. M. Asiri and M. K. Nazeeruddin, *ChemSusChem*, 2016, **9**, 10–27.
14 Y. Wang, Y. Yue, X. Yang and L. Han, *Adv. Energy Mater.*, 2018, **8**, 1800249.
15 X. Zhao and M. Wang, *Mater. Today Energy*, 2018, **7**, 208–220.
16 T. P. I. Saragi, T. Spehr, A. Siebert, T. Fuhrmann-Lieker and J. Salbeck, *Chem. Rev.*, 2007, 107, 1011–1065.
17 A. Binek, M. L. Petrus, N. Huber, H. Bristow, Y. Hu, T. Bein and P. Docampo, *ACS Appl. Mater. Interfaces*, 2016, **8**, 12881–12886.
18 M. L. Petrus, T. Bein, T. J. Dingemans and P. Docampo, *J. Mater. Chem. A*, 2015, **3**, 12159–12162.
19 M. L. Petrus, M. T. Sirtl, A. C. Closs, T. Bein and P. Docampo, *Mol. Syst. Des. Eng.*, 2018, **3**, 734–740.
20 R. Tiazkis, S. Paek, M. Daskeviciene, T. Malinauskas, M. Saliba, J.

Nekrasovas, V. Jankauskas, S. Ahmad, V. Getautis and M. Khaja Nazeeruddin, *Sci. Rep.*, 2017, **7**, 150.

21 T. Malinauskas, M. Saliba, T. Matsui, M. Daskeviciene, S. Urnikaite, P. Gratia, R. Send, H. Wonneberger, I. Bruder, M. Graetzel, V. Getautis and M. K. Nazeeruddin, *Energy Environ. Sci.*, 2016, **9**, 1681–1686.

22 K. Rakstys, M. Saliba, P. Gao, P. Gratia, E. Kamarauskas, S. Paek, V. Jankauskas and M. K. Nazeeruddin, *Angew. Chemie*, 2016, **128**, 7590–7594.

23 M. Maciejczyk, A. Ivaturi and N. Robertson, *J. Mater. Chem. A*, 2016, **4**, 4855–4863.

24 B. Xu, D. Bi, Y. Hua, P. Liu, M. Cheng, M. Grätzel, L. Kloo, A. Hagfeldt and L. Sun, *Energy Environ. Sci.*, 2016, **9**, 873–877.

25 D. Bi, B. Xu, P. Gao, L. Sun, M. Grätzel and A. Hagfeldt, *Nano Energy*, 2016, **23**, 138–144.

26 P. Gratia, A. Magomedov, T. Malinauskas, M. Daskeviciene, A. Abate, S. Ahmad, M. Grätzel, V. Getautis and M. K. Nazeeruddin, *Angew. Chemie Int. Ed.*, 2015, **54**, 11409–11413.

27 A. Magomedov, N. Sakai, E. Kamarauskas, G. Jokubauskaitė, M. Franckevičius, V. Jankauskas, H. J. Snaith and V. Getautis, *Chem. - An Asian J.*, 2017, **12**, 958–962.

28 Š. Daškevičiū tė, N. Sakai, M. Franckevičius, M. Daškevičienė, A. Magomedov, V. Jankauskas, H. J. Snaith and V. Getautis, *Adv. Sci.*, 2018, **5**, 1700811.

29 M. Daskeviciene, S. Paek, Z. Wang, T. Malinauskas, G. Jokubauskaite, K. Rakstys, K. T. Cho, A. Magomedov, V. Jankauskas, S. Ahmad, H. J. Snaith, V. Getautis and M. K. Nazeeruddin, *Nano Energy*, 2017, **32**, 551–557.

30 P. Agarwala and D. Kabra, *J. Mater. Chem. A*, 2017, **5**, 1348–1373.

31 M. Saliba, T. Matsui, J.-Y. Seo, K. Domanski, J.-P. Correa-Baena, M. K. Nazeeruddin, S. M. Zakeeruddin, W. Tress, A. Abate, A. Hagfeldt and M. Grätzel, *Energy Environ. Sci.*, 2016, **9**, 1989–1997.

32 G. Cook, *Enamines : Synthesis: Structure, and Reactions, Second Edition.*, Routledge, 2 edition., 1987.

33 M. J. Frisch, G. W. Trucks, H. B. Schlegel, G. E. Scuseria, M. A. Robb, J. R. Cheeseman, G. Scalmani, V. Barone, B. Mennucci, G. A. Petersson, H. Nakatsuji, M. Caricato, X. Li, H. P. Hratchian, A. F. Izmaylov, J. Bloino, G. Zheng, J. L. Sonnenberg, M. Hada, M. Ehara, K. Toyota, R. Fukuda, J. Hasegawa, M. Ishida, T. Nakajima, Y. Honda, O. Kitao, H. Nakai, T. Vreven, J. A. Montgomery Jr., J. E. Peralta, F. Ogliaro, M. Bearpark, J. J. Heyd, E. Brothers, K. N. Kudin, V. N. Staroverov, T. Keith, R. Kobayashi, J. Normand, K. Raghavachari, A. Rendell, J. C. Burant, S. S. Iyengar, J. Tomasi, M. Cossi, N. Rega, J. M. Millam, M. Klene, J. E. Knox, J. B. Cross, V. Bakken, C. Adamo, J. Jaramillo, R. Gomperts, R. E. Stratmann, O. Yazyev, A. J. Austin, R. Cammi, C. Pomelli, J. W. Ochterski, R. L. Martin, K. Morokuma, V. G. Zakrzewski, G. A. Voth, P. Salvador, J. J. Dannenberg, S. Dapprich, A. D. Daniels, O. Farkas, J. B. Foresman, J. V. Ortiz, J. Cioslowski, D. J. Fox, Gaussian 09, Revision D.01, Gaussian, Inc., Wallingford, CT 2013.

34 T. Malinauskas, D. Tomkute-Luksiene, R. Sens, M. Daskeviciene, R. Send, H. Wonneberger, V. Jankauskas, I. Bruder and V. Getautis, *ACS Appl. Mater. Interfaces*, 2015, **7**, 11107–11116.

35 D. Vaitukaityte, Z. Wang, T. Malinauskas, A. Magomedov, G. Bubniene, V. Jankauskas, V. Getautis and H. J. Snaith, *Adv. Mater.*, 2018, 1803735.